Journal Pre-proofs

SIZE SHIFTING OF SOLID LIPID NANOPARTICLE SYSTEM TRIGGERED BY ALKALINE PHOSPHATASE FOR SITE SPECIFIC MUCOSAL DRUG DELIVERY

Bao Le-Vinh, Christian Steinbring, Richard Wibel, Julian David Friedl, Andreas Bernkop-Schnürch

PII: S0939-6411(21)00079-5
DOI: https://doi.org/10.1016/j.ejpb.2021.03.012
Reference: EJPB 13540

To appear in: *European Journal of Pharmaceutics and Biopharmaceutics*

Received Date: 3 November 2020
Revised Date: 16 March 2021
Accepted Date: 20 March 2021

Please cite this article as: B. Le-Vinh, C. Steinbring, R. Wibel, J. David Friedl, A. Bernkop-Schnürch, SIZE SHIFTING OF SOLID LIPID NANOPARTICLE SYSTEM TRIGGERED BY ALKALINE PHOSPHATASE FOR SITE SPECIFIC MUCOSAL DRUG DELIVERY, *European Journal of Pharmaceutics and Biopharmaceutics* (2021), doi: https://doi.org/10.1016/j.ejpb.2021.03.012

SIZE SHIFTING OF SOLID LIPID NANOPARTICLE SYSTEM TRIGGERED BY ALKALINE PHOSPHATASE FOR SITE SPECIFIC MUCOSAL DRUG DELIVERY

Bao Le-Vinh[1,2], Christian Steinbring[1], Richard Wibel[1], Julian David Friedl[1], Andreas Bernkop-Schnürch[1,*]

[1] Department of Pharmaceutical Technology, Institute of Pharmacy, University of Innsbruck, Innrain 80/82, 6020 Innsbruck, Austria

[2] Department of Industrial Pharmacy, Faculty of Pharmacy, University of Medicine and Pharmacy at Ho Chi Minh city, 700000 Ho Chi Minh city, Vietnam

Keywords: size shifting, size changing, mucosal drug delivery, mucus permeation, solid lipid nanoparticles, alkaline phosphatase, phosphate ester surfactant, phosphorylated PEG surfactant, interparticle aggregation.

*Corresponding author:

Department of Pharmaceutical Technology,

Institute of Pharmacy, University of Innsbruck

Innrain 80/82, 6020 Innsbruck, Austria

Tel.: +43-512-507 58601 30. Fax: +43-512-507 58699

E-mail: andreas.bernkop@uibk.ac.at

Abstract

We aim to prepare a size-shifting nanocarrier for site-targeting mucosal drug delivery that can penetrate through mucus gel layer and remain close to the absorption membrane. As nanocarriers can be engineered to penetrate mucus but they can also back diffuse into outer mucus regions, a size shifting to micron range once they have reached the absorption membrane would prevent back-diffusion effect and extend drug release over a long period of time. For this purpose, we loaded solid lipid nanoparticles (SLN) with a phosphate ester surfactant and octadecylamine. Alkaline phosphatase (AP), a membrane bound enzyme was for the first time utilized as an in situ partner for triggering the size conversion at epithelial cell surface. Having the size of ~120 nm, SLN with hydrophilic and phosphate-decorated shells were shown to penetrate through mucus gel and form aggregates above cell layer surface. Aggregates of 5-8 μm were formed due to interparticle interactions induced by enzymatic phosphate removal after ~30 min in contact with isolated AP. The developed SLN system could be a potential tool for mucosal drug delivery to AP-expressing tissues like colon, lung, cervix, vagina and some mucus-secreting tumors.

Graphical abstract

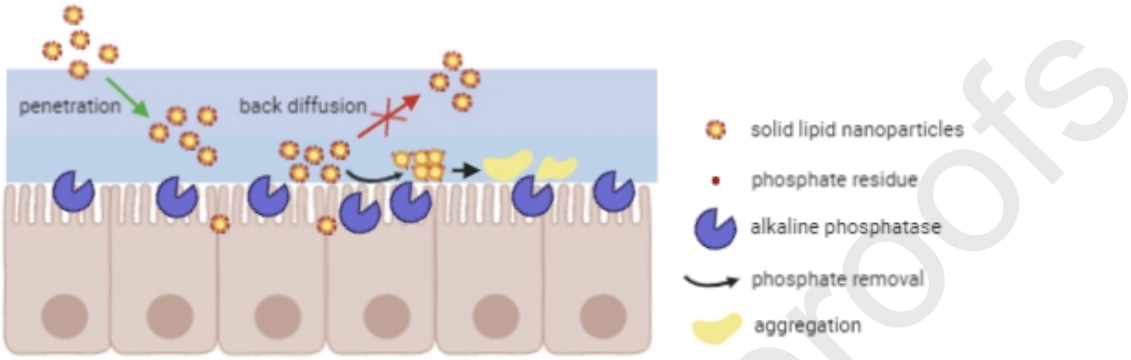

1. Introduction

Mucus layer, a viscoelastic and adhesive gel that covers mucosal surfaces remains a tough barrier for drug delivery. It is mainly constructed by cross-linked and entangled mucins forming a three-dimensional network with average pore size in the range of 20-300 nm [1,2]. Beside steric obstruction, the mucus gel barrier traps foreign particles by various mechanisms including hydrophobic interactions and electrostatic interactions [3]. Particles larger than 500 nm are mostly immobile in mucus and even smaller particles exhibit sufficiently high mucus permeating properties only when they are decorated with PEG [1], sulfate, or carboxylate substructures [4]; contain bile salts or mucolytic enzymes on their surfaces [5–7]; or are engineered to have virus-mimicking surfaces [8]. Driven by a concentration gradient towards the membrane, mucus-permeating nanoparticles diffuse through the mucus network reaching the underlying epithelium. As soon as this concentration gradient is not anymore available, however, these particles do not remain on the epithelium and tend to back-diffuse into outer mucus regions. The time window for a targeted drug release directly at the absorption membrane is thus on many mucosal tissues too short to gain a therapeutic benefit. It was therefore the aim of this study to design mucus permeating nanocarriers that remain close to the absorption membrane once they have reached it.

The concept to achieve this goal is based on the design of size-shifting nanocarriers that can change their size from nano- to micro- range directly at the absorption membrane. Particles have to be in nano-size range with hydrophilic and negatively charged surface that would help them to permeate the mucus gel layer effectively. Having reached the epithelial surface, these nanoparticles should aggregate triggered by an in situ factor. Because of the large size of these aggregates, their mobility and diffusivity is minimized so that they remain longer in the adherent mucus close to the epithelial surface where they can act as drug depots and slowly unload their cargoes. Localized treatments of diseases like ulcerative colitis, Crohn's disease, vaginal infections or pulmonary diseases would also benefit from this approach.

Solid lipid nanoparticles (SLN) have been widely studied as promising carriers for mucosal drug delivery such as oral, intraoral, pulmonary, nasal, vaginal, ocular and intravesical drug delivery [9–12]. They are

composed of biocompatible solid lipids like triglycerides, fatty alcohols, and waxes being generally regarded as safe that are stabilized by surfactants. With their versatility in surface engineering and cargo loading, we exploited SLN as carriers for this size-shifting concept. To make SLN in situ size shifting, alkaline phosphatase (AP), which has recently been exploited as a reliable partner for smart drug delivery nanosystems [13,14] was utilized. This is a membrane bound enzyme expressed on epithelial cells of various mucosal membranes lining the gastrointestinal (GI), respiratory or vaginal tract [15–17]. Hence, we first loaded SLN with a phosphate ester surfactant and the fatty amine octadecylamine in appropriate ratios. The phosphate ester surfactant was used to provide a negatively charged phosphate-decorated shell to foster mucus permeation [18,19]. Once getting into contact with AP, phosphates are gradually removed from SLN outer shells making particles' charges less negative and exposing the positively charged octadecylamine residues. This results in a decrease of interparticle repulsion and an increase of interparticle electrostatic interactions leading to the aggregation of SLN as illustrated in Figure 1.

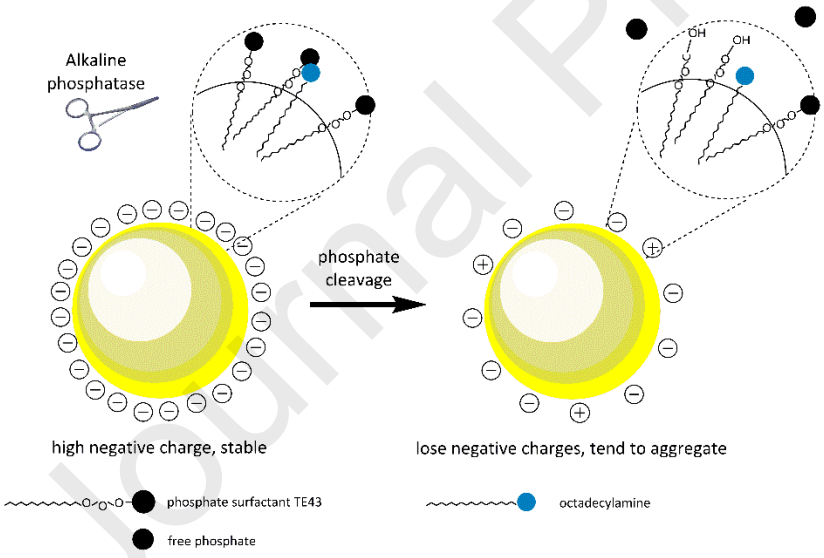

Figure 1. Proposed mechanism of solid lipid particles aggregation triggered by alkaline phosphatase.

2. Materials and methods

2.1. Materials

Lanphos TE43 (phosphorylated PEG surfactant) was kindly provided by Lankem, UK. This is a phosphate ester (C12-15 + 3EO) in acid form, mainly monoester, and dispersible in water. Geleol™ (glyceryl

monostearate) melting range 54-64 °C was kindly provided by Gattefossé, Germany. Lutrol® F68 (poloxamer 188) was obtained from BASF, Germany. Span® 60 (sorbitan monostearate), 1-butanol, octadecylamine, malachite green (MLG), ammonium molypdate, minimum essential medium (MEM), MEM Eagle powder, HEPES, isolated AP from bovine intestinal mucosa (≥2,000 DEA units/mg protein) and phosphatase inhibitor cocktail 2 (PIC2) were purchased from Sigma-Aldrich, Austria. Fetal bovine serum FBS superior was purchased from Biochrom GmbH, Germany. Penicillin-Streptomycin solution (Penicillin 10 000 U/mL and Streptomycin 10 mg/mL) was obtained from Pan Biotech, Germany.

Caco-2 cell line was obtained from European Collection of Authenticated Cell Cultures (ECACC, Health Protection Agency, Salisbury, Wiltshire, UK). Cells at passage numbers of 25-30 were used. Cell culture medium was MEM supplemented with 10% heat inactive FBS and 1% penicillin-streptomycin solution. Phenol red free medium (PFM) and HEPES buffered saline (HBS) were used in phosphate release and cell related experiments. PFM was comprised of 9.3 g/L MEM Eagle powder, 0.292 g/L L-glutamine and 2.2 g/L sodium bicarbonate. HBS was comprised of 1 g/L dextrose, 20 mM HEPES, 5 mM KCl, 136.7 mM NaCl and 1 mM $CaCl_2$; the pH was adjusted to 7.4 with 5 M NaOH. The reconstituted media were sterilized by 0.22 µm filtration under LAF hood and stored at 4°C for further use.

2.2. Preparation and characterization of SLN

SLN was prepared by ultrasound dispersing technique. Lipid phase and aqueous phase (Table 1) were heated and kept at 75 °C. The latter was added to the former under shaking at 900 rpm (ThermoMixer C, Eppendorf, Germany). The formed coarse emulsion was sonicated with a probe sonicator (Hielscher UP200H, Germany) for three cycles to obtain a nanoemulsion. Each cycle was 30 s sonicating at 60 W and 30 s resting. Afterwards, hot nanoemulsion was cooled down on ice facilitating lipid crystallization. SLN was then filtered through a cellulose filter (Rotilabo 113P, Carl Roth, Germany; particle retention 5-8 µm).

Table 1. Formulation of solid lipid nanoparticles (SLN).

Lipid phase	
Glyceryl monostearate	200 mg
Sorbitan monostearate	60 mg
Octadecylamine	5 mg
Phosphorylated PEG surfactant	60 mg
Butanol	500 µL
Lumogen red*	1 mg
Aqueous phase	
Poloxamer 188	100 mg
Water	10 mL

*: Lumogen red is added to sample for observation under confocal microscopy.

SLN size and polydispersity index (PdI) were measured utilizing dynamic light scattering (Zetasizer Nano ZSP, Malvern Panalytical, UK) with backscatter detection mode. For this purpose, SLN was diluted 20 times in HBS. Zeta potential (ZP) was measured using a Dip cell (Malvern ZEN 1002) after a 20-fold further dilution with water. SLN was stored at room temperature. Changes in size and ZP of SLN and diluted SLN were observed within 48 h.

2.3. Cytotoxicity of SLN components and SLN

Caco-2 cell line derived from human colon was used to assess the cytotoxicity of SLN with resazurin test. Caco-2 cells were seeded on a 96-well plate at a density of $6x10^4$ cells/cm^2. Cells were cultured for three days in a cell incubator adjusted at 37 ^oC, 95% humidity and 5% CO_2. On the test day, cell culture medium was replaced with PFM and cells were incubated for 30 min. Subsequently, PFM was replaced with 100 µL of test sample solution prepared in PFM and cells were incubated for 3 h and 24 h. Phosphorylated PEG surfactant and sorbitan monostearate at 6, 60 and 600 ppm were tested, while octadecylamine was prepared as saturated solution due to its poor aqueous solubility. Saturated concentration of octadecylamine in HBS is 55 ± 12 µM determined by 2,4,6-trinitrobenzene sulfonic acid (TNBS) assay [20]. Cytotoxicity of SLN was tested at various dilution levels of 10x, 50x, 100x and 1000x. Triton X-100 (0.5% w/v) and PFM served as positive and negative control, respectively. At the end of testing time, test samples were removed and cells were washed with PFM. To each well 100 µL of 44 µM resazurin solution dissolved in PFM was added and cells were further incubated for 2 h. The supernatants were then transferred to a

96-well microplate and their fluorescence intensities were measured using a microplate reader (Tecan Spark, Austria) at λ_{ex} of 540 nm and λ_{em} of 590 nm. Cell viability rates were calculated according to equation (1):

Cell viability (%) = Fs x 100 / Fc (Eq. 1)

where Fs and Fc are the fluorescence intensity of sample and negative control, respectively.

2.4. Phosphate release and size changing induced by phosphate removal

To investigate the ability of AP to cleave phosphate from SLN and induce a size change, diluted SLN was incubated with isolated AP. Furthermore, SLN was added on Caco-2 cell layer expressing membrane bound AP to see whether similar effects occur.

2.4.1. Phosphate release and size increase by isolated AP

SLN was diluted 100 times with HBS. Afterwards, five µL of 1000 U/mL isolated AP stock solution was added to 10 mL of diluted SLN. There were two control samples: the first one was diluted SLN without adding enzyme and the second one was diluted SLN with the same amount of isolated AP and 0.5% v/v of PIC2. The samples were incubated at 37 °C and 300 rpm (Thermomixer C, Eppendorf, Germany). For phosphate release study, fifty µL of sample was withdrawn at predetermined time points of 5, 15, 30, 45, 60, 90, 120 and 180 min. Each aliquot was transferred to a 96-well microtiter plate and 5 µL of 3.6 M H_2SO_4 was added to stop enzyme activity. Released phosphate was quantified by MLG assay as described in section 2.4.3. During experiment time, size and ZP were also monitored with the Zetasizer Nano ZSP. For ZP measurement, sample was diluted 20 times with water to keep conductivity at ~ 1mS/cm.

To monitor the change of particle size continuously, SLN was diluted 20 times in HBS and 2 mL of sample spiked with 2 U of isolated AP was transferred to a disposable cuvette and incubated at 37 °C in the Zetasizer. Size measurement took place every 1 min. In order to confirm the role of phosphorylated PEG surfactant in size changing, a SLN formulation without phosphorylated PEG surfactant was prepared. This formulation was also diluted 20 times in HBS, mixed with the same amount of isolated AP and size was measured over time.

Furthermore, effects of different concentrations of isolated AP and PIC2 on phosphate release from SLN were evaluated. Accordingly, SLN diluted at 1:100 in HBS was incubated with isolated AP in final concentrations of 0.01, 0.1, 0.5 and 1 U/mL. At the isolated AP concentration of 0.5 U/mL, different concentrations of PICs (0.1, 0.5, 1 and 2% v/v) were added to test samples. Aliquots of 50 µL were withdrawn at predetermined time points of 5, 15, 30, 60, 90, 120, 180 and 240 min. Sample treatment was done as described above. All experiments were performed in triplicate.

2.4.2. Phosphate release on Caco-2 cell layer

Caco-2 cells are able to differentiate into a monolayer of cells with many properties mimicking the brush border layer found in the human intestine and they also express membrane bound AP. Caco-2 cells were seeded on a 24-well plate at a density of $1x10^4$ cells/cm^2. Cells were cultured for 14 days at 37 ^oC in an atmosphere of 95% humidity and 5% CO_2. We performed the phosphate release experiments in the absence and presence of phosphatase inhibitors. On the test day, culture medium was removed and cell layer was washed twice with prewarmed HBS. Afterwards, cells were divided in two groups and incubated for 30 min with HBS or 0.5% v/v PIC2 in HBS. At the end of the incubation time, medium was replaced with 700 µL of 500 times diluted SLN in HBS. PIC2 at 0.5% was added to inhibit phosphatase activity. At predetermined time points of 0, 15, 30, 45, 60, 90, 120 and 180 min, fifty µL of sample was aliquoted in 96-well microtiter plate and mixed with 5 µL of 3.6 M H_2SO_4. Freed phosphate was quantitatively determined by MLG assay as described in section 2.4.3.

2.4.3. MLG assay

MLG assay was utilized to determine the free inorganic phosphate amount. MLG reagent was freshly prepared by mixing 10 mL of 0.15% MLG in 3.6 M H_2SO_4, 400 µL of 11% Triton X100 and 6 mL of 8% ammonium molybdate. For the assay, 100 µL of MLG reagent was added to 50 µL of sample and mixture was incubated for 15 min. Afterwards, absorbance at 630 nm was recorded using the Tecan microplate reader. A standard curve was constructed from a series of 3-200 µM KH_2PO_4 solution and 5 µL of 3.6 M H_2SO_4 was added to each 50 µL of the standard solution.

2.5. SLN size change on Caco-2 cell layers

For these experiments, SLN was loaded with a fluorescent dye, Lumogen red at 0.5% w/w to the solid lipid. Samples were observed with a confocal laser scanning microscope (CLSM).

2.5.1. Observation on cell layers

Caco-2 cells were seeded on an Ibidi µ-slide 8 well at cell density of $1x10^4$ cells/cm^2 and cultured for 14 days. Prior to the test, cells were washed with HBS and then incubated with 200 µL of 100-fold diluted SLN in HBS for 1 h. Control wells were incubated with SLN diluted in HBS supplemented with 0.5% v/v PIC2.

2.5.2. Observation on cell layers covered with mucus

Porcine mucus was taken from intestines of freshly slaughtered pigs from a local abattoir following previously described protocols [21,22] with some modifications to ensure cell compatibility. The wall of the small intestine was incised longitudinally and gently scraped in one direction with a silicon scraper to collect both adherent and non-adherent mucus. Mucus was purified with an extraction solution composed of 0.9% sodium chloride and protease inhibitor cocktail (cOmplete Protease Inhibitor Tablets, Roche; 1 tablet per 50 mL). To remove debris, 5 mL of extraction solution was added to 1 g of crude mucus and gently stirred (< 40 rpm) for 1 h at 4 °C. The gentle agitation was to limit the disruption of mucus gel and allowed the debris to settle. The cleaner portion of the mucus was centrifuged at 10 400 g for 2 h at 10 °C (Sigma 3-18KS, 19776-H rotor, Germany). The supernatant was discarded and only the upper clean mucus was carefully collected leaving the debris at the bottom of the centrifuge tube. The purification process was repeated twice using HBS instead of extraction solution. Thereafter, the clean intestinal mucus was stored at −20 °C until further use.

Caco-2 cells were seeded on an Ibidi µ-slide 18 well at cell density of $1x10^4$ cells/cm^2 and cultured for 14 days. The Ibidi µ-slide 18 well had a growth area/well of 34 mm^2. On the test day, cells were washed with HBS and buffer was removed. Subsequently, cell layer was covered with mucus by carefully spreading of 30 µL of mucus onto the layer. With this mucus amount, calculated thickness of mucus layer above the cell layer was ~ 800 µm. The µ-slide was incubated for 30 min followed by addition of 70 µL of 100-fold diluted

SLN in HBS and incubating for 1 h. Control wells were incubated with SLN diluted in HBS supplemented with 0.8% v/v PIC2.

2.5.3. Image processing

In order to study the influence of AP on the aggregation behavior of fluorescent SLN, CLSM (Leica TCS SP8) with the appropriate filter sets was used to record z-stacks with 0.2 µm z-step length. All fluorescence images were recorded under equal confocal settings. Image post processing (3D Gaussian filter) and analysis was performed utilizing the open source image processing and analysis platform ImageJ. Furthermore, Ilastik, a machine-learning based segmentation toolkit, was used for identification, segmentation and size determination of the aggregated fluorescent SLN; the calculated object feature size data, given in pixel, were further analyzed and displayed with MatLab.

The raw and segmented image data of the SLN are displayed (Figure 10A-C) either as maximum projections of the image volume along the y-direction of the stack (A: segmented data, above the cell layer; C: raw data, including the cell layer) or as 3D-rendered image (B: the segmented data; other 3D display: aggregates above the cell layer, not segmented). Cellular internalization of SLN is displayed by maximum projections along the z direction of the cell-layer prepared from 10 images of the image stack. The corresponding SLN aggregates above the cell layer are also shown in 3D.

2.6. Drug release

To investigate the effect of enzyme-triggered aggregation of SLN on drug release, we loaded curcumin as a model drug in SLN at 0.5% w/w based on lipid amount. The exact amount of curcumin was dissolved in melted lipid phase and curcumin loaded SLN (SLN-C) was prepared as described in section 2.2. The entrapment efficiency (EE) was calculated by equation (2):

EE = (Loaded drug – free drug) x 100 / Loaded drug (Eq. 2)

Free drug in undiluted SLN-C was evaluated after SLN extraction by a centrifugal filter device with molecular weight cut-off (MWCO) of 30 kDa (Amicon Ultra 15 mL, Merck Millipore).

We used a dialysis bag setup to explore the drug release from SLN-C in absence and presence of isolated AP. Accordingly, dialysis sac with MWCO of 14 kDa (Sigma D9927) was filled with 1.5 mL of 20 times diluted SLN-C in HBS. For enzymatic aggregation, isolated AP was added at a concentration of 1 U/mL. The dialysis sac was then put in a 50-mL tube and soaked in 35 mL of 15% ethanol in HBS. Ethanol was used to facilitate curcumin dissolution, ensuring sink conditions. Experiments were performed in triplicate. Sample tubes were kept at 37 ^{o}C and shaken at 600 rpm (Thermomixer C, Eppendorf, Germany). At predetermined time points, 100 µL of sample was withdrawn and compensated with the same amount of fresh medium.

Samples were quantitatively determined by fluorescence assay, reading at excitation and emission wavelength of 420 nm/550 nm (Tecan Spark, Austria). Amount of curcumin was calculated based on a standard curve of curcumin in 15% ethanol in HBS. The standard curve was in the range of 0.001-1 µg/mL.

2.7. Statistical analysis

Statistical analysis was performed using Microsoft Excel 2016. Data were shown as mean and standard deviation (SD) in parentheses. Student's t-test was used to assess the significance of difference between two means.

3. Results and discussion

3.1. Preparation and characterization of SLN

Size, PdI and ZP of SLN diluted in HBS are reported in Table 2. ZP of SLN measured in water was -45.4 (2.1) mV. The formulation was stable within 2-day storage at room temperature. After two days, there was no significant change in size, PdI and ZP compared to day-0 values ($p>0.05$). Loading of 0.5% Lumogen red or curcumin did not cause significant changes in size, PdI and ZP.

SLN without phosphorylated PEG surfactant were prepared to evaluate the effect of phosphorylated PEG surfactant on SLN properties and in particular on the AP-mediated aggregation process. This control SLN had a smaller size of 74.9 (1.5) nm with a narrower distribution and a slightly positive charge. The incorporation of phosphorylated PEG surfactant or curcumin into SLN formulation can increase the

lipophilicity of the lipid phase leading to the bigger size of SLN [23,24]. Besides, the melted lipid phase became more viscous in the presence of phosphorylated PEG surfactant so that more input energy might have been required to obtain the same small size as for control SLN.

Table 2. Characterization of solid lipid nanoparticles (SLN). Particle size was measured after dilution 20 times in HBS. Zeta potential (ZP) was measured after a 20 times further dilution with water. Indicated values are means and SDs in parentheses (n ≥ 3).

	SLN	SLN after 48 h	SLN without phosphorylated PEG surfactant	SLN-C*
Size (nm)	126.4 (3.5)	127.4 (3.4)	74.9 (1.5)	131.1 (1.9)
PdI	0.23 (0.02)	0.24 (0.02)	0.13 (0.001)	0.24 (0.01)
ZP (mV)	-27.9 (1.3)	-28.7 (0.3)	7.3 (2.6)	-26.2 (4.9)

(*) SLN-C: curcumin loaded solid lipid nanoparticles

SLN was stabilized by a mixture of phosphorylated PEG surfactant, the high molecular mass polymeric surfactant poloxamer 188 with a HLB of 29 and the low molecular mass sorbitan monostearate with a HLB of 6. The combination of emulsifiers has been shown to ease the emulsification process and to stabilize emulsions [24,25]. Co-surfactants like butanol can make the oil-water interface flexible and can lower interfacial tension [26]. It has been demonstrated that an insufficient coverage of the particle surface by hydrophilic substructures of surfactants may lead to pronounced hydrophobic interactions between the oily core of particles and hydrophobic domains of mucins [4]. A combination of different types of surfactants, however, will contribute to a densely packed hydrophilic surface of SLN and thus reduce hydrophobic interactions with the mucus gel network.

Poloxamer 188 was used as the main surfactant for SLN formation and stabilization. The critical micelle concentration (CMC) of poloxamer 188 is not well defined and values are depending on the utilized method [27]. Consequently different CMC values for poloxamer 188 were reported such as 24-32 mg/mL [28] and 12.5–51.7 mg/mL [29]. In order to minimize the formation of micelles, poloxamer 188 was used in a concentration of 10 mg/mL (

Table 1) in SLN formulation that is below most of reported CMC values.

Because of the hydrophilic PEG-spacer between the phosphate group and the lipophilic aliphatic tail, this phosphate substructure is likely located in outer regions of the hydrophilic corona of SLN being more easily accessible for AP. Octadecylamine is a fatty amine with logP of 7.7 and pK_a of 10.6. The presence of octadecylamine on SLN surface provides a slightly positive ZP as shown in Table 2. Although it is generally known that the coexistence of cationic and anionic surfactants poses a risk to precipitation or instability, this is not always the case [30,31]. Herein, the combination of phosphorylated PEG surfactant and octadecylamine in the same formulation did not cause precipitation and SLNs were stable for at least 48 h. Due to electrostatic interactions, a pseudo zwitterionic surfactant might be temporarily formed showing an increase in the volume of the hydrophobic tail and a relative decrease in the size of the hydrophilic head [30].

3.2. Cytotoxicity of SLN

Cytotoxicity of excipients and of SLN at various concentrations on Caco-2 cells is displayed in Figure 2. Sorbitan monostearate and octadecylamine did not show a toxic effect to cells within 24 h of incubation at tested concentrations, whereas phosphorylated PEG surfactant was cytotoxic in a time- and dose-dependent manner. Higher dilutions of SLN were less harmful to cells and dilution levels higher than 1:100 appeared to be safe. SLN dilution of 1:10 contained the same final phosphorylated PEG surfactant concentration as 600 ppm phosphorylated PEG surfactant solution. However, cell viability upon incubation with SLN 1:10 was significantly higher than that of 600 ppm phosphorylated PEG surfactant solution ($p<0.01$), i.e. 48 (4) % and 1.2 (0.8) %, respectively. Immobilizing the phosphorylated PEG surfactant on SLN reduced obviously its cytotoxicity.

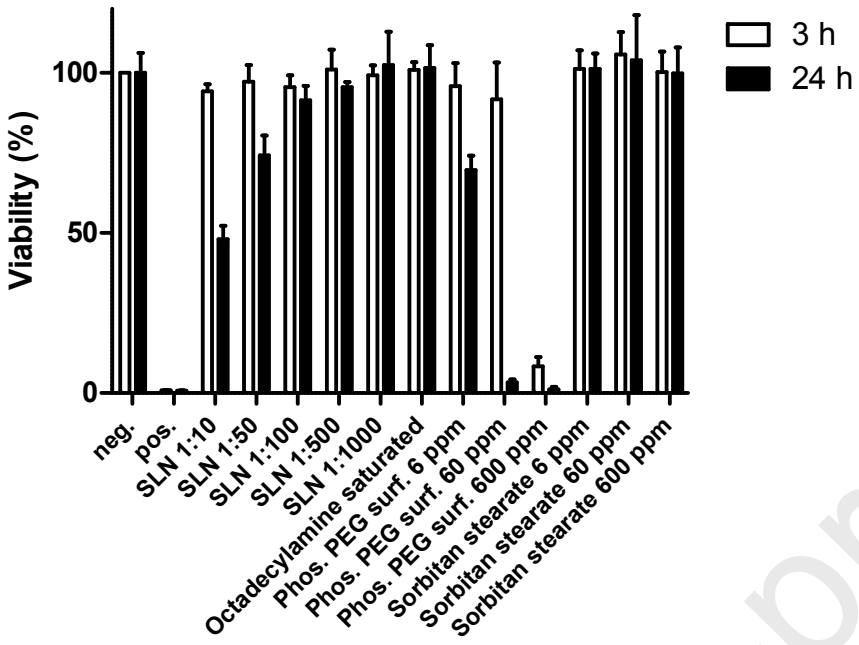

Figure 2. Viability of Caco-2 cells after incubation with diluted SLN and excipients used for the preparation of SLN at indicated concentrations. Positive control was 0.5 % w/v Triton X100. Indicated values are means and SDs (n=3). Phos. PEG surf. = Phosphorylated PEG surfactant.

3.3. Phosphate release inducing size and ZP changes

Phosphate release from SLN increased over time and likely reached a plateau phase after 120 min (Figure 3). Phosphate release induced a change in ZP as shown in Figure 4 with an increase of Δ6 mV within 15 min. The ZP would have continued to increase due to the continuous phosphate cleavage (Figure 3) but it decreased from time point 45 min on. At this time point, a change in size due to aggregation of SLN was observed explaining decline in ZP as the increase in particle size diminished the electrophoretic mobility of SLN. PIC2 at 0.5% v/v did not entirely inhibit enzyme activity resulting in a lower amount of released inorganic phosphates (Figure 3). Nonetheless, we found this PIC2 concentration safe to cells in phosphate release experiments on cell layers. In the presence of PIC2, ZP slightly increased within 45 min (Figure 4) and no aggregation was observed during this test period. Control samples without isolated AP did not show significant phosphate release and ZP change.

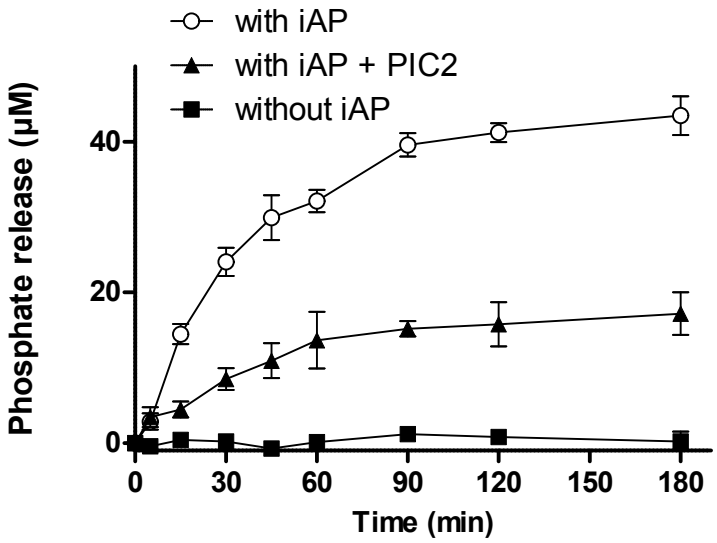

Figure 3. Phosphate release from SLN at 1:100 dilution in HBS upon incubation with 0.5 U/mL isolated AP, with 0.5 U/mL isolated AP and 0.5% v/v phosphatase inhibitors, and without isolated AP. Indicated values are means and SDs (n=3). iAP = isolated AP.

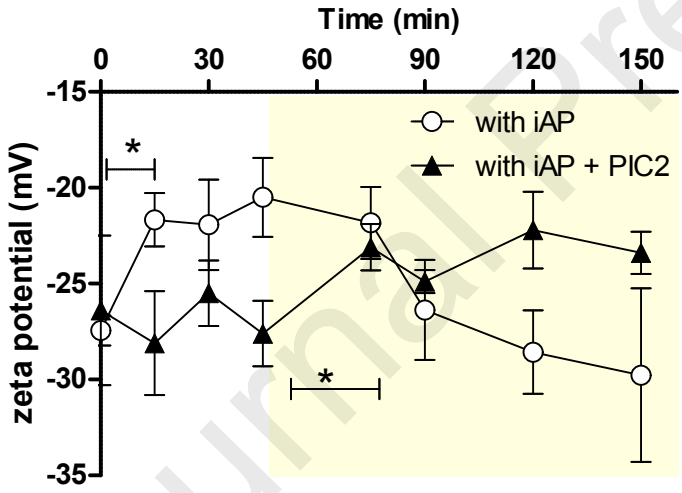

Figure 4. Change of SLN zeta potential upon incubation with 0.5 U/mL isolated AP (iAP), without or with the presence of 0.5% PIC2. SLN was diluted 1:100 in HBS. Yellow region: aggregation occurred in sample without PIC2, electrophoretic mobility of particles might have changed. Indicated values are means and SDs (n=3). (*) significant difference $p < 0.05$.

The effect of isolated AP and PIC2 on phosphate release is illustrated in Figure 5. Higher concentrations of isolated AP led to higher release of phosphate showing that there was a surplus of substrate in all experiments. A comparatively fast release took place within the first 30 min. Already released phosphate inhibited AP in a competitive manner and slowed down the release kinetic. According to these results, SLN aggregation will strongly depend on AP expression at targeted tissues. As shown in Figure 5B, the

concentration of 0.1% v/v PIC2 was sufficient to inhibit ~50% AP activity. The inhibitory effect was greater at higher concentrations of PIC2, although a complete inhibition was not reached. The reason might be the shallow active site of AP making it difficult for inhibitors to provide complete inhibition [32].

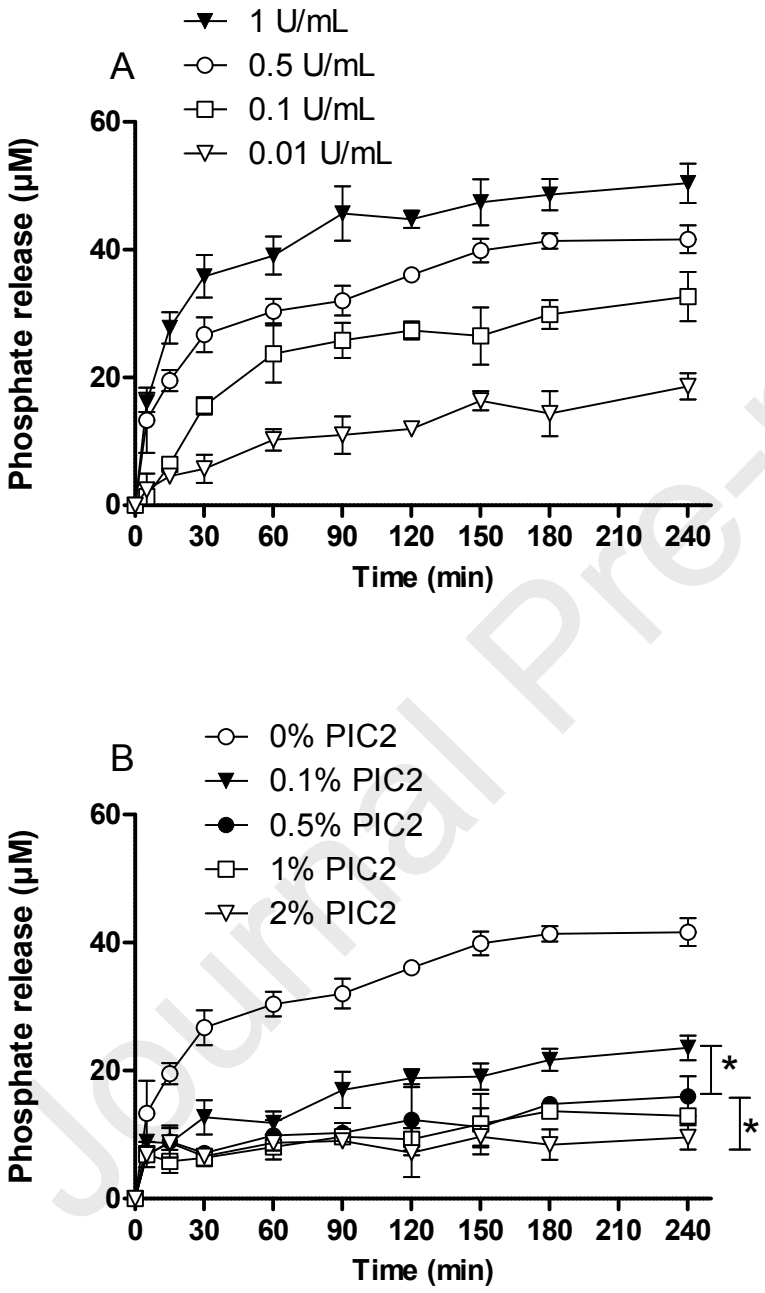

Figure 5. (A) Phosphate release from SLN at 1:100 dilution in HBS upon incubation with isolated AP in final concentrations of 0.01, 0.1, 0.5 and 1 U/mL. (B) Phosphate release from SLN at 1:100 dilution in HBS incubated with 0.5 U/mL isolated AP and PIC2 in final concentrations of 0.1, 0.5, 1 and 2% v/v PIC2. Indicated values are means and SDs (n=3), (*) significant difference p < 0.05.

Along with phosphate release and ZP change, SLN size increased in the presence of the enzyme. As displayed in Figure 6 (top), size started increasing from measurement no. 20 on, that was performed ~ 30 min after the addition of the enzyme. An intensity-weighted size peak of 1200 nm was reached at measurement no. 33 (50 min) followed by a drop. This was due to less backward scattered photons caused by the formation of oversized aggregates making an accurate particle size analysis impossible. This effect was accompanied by the falling of derived count rate. At this stage, SLN aggregates were already visible to naked eyes. By forward light scattering setting, Z-average size of 6072 (1072) nm and PdI of 1.0 was recorded. The control sample without isolated AP and control sample of SLN without phosphorylated PEG surfactant incubated with isolated AP did not show any size change during observation time (Figure 6. middle and bottom). This confirmed roles of phosphorylated PEG surfactant and isolated AP as key factors in the size change.

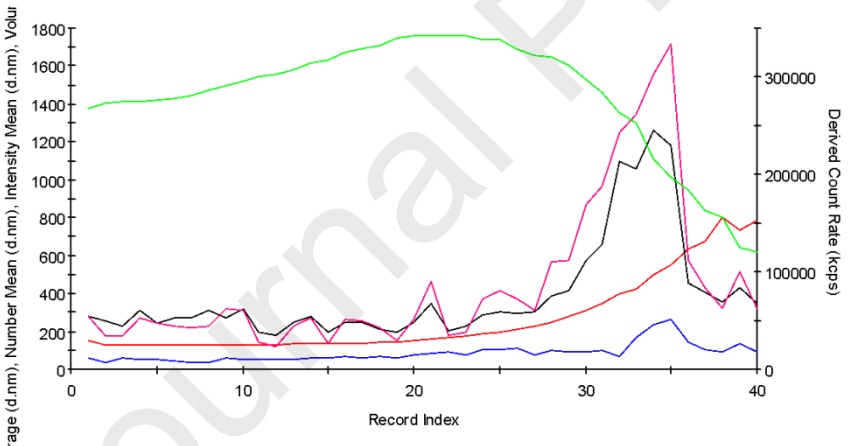

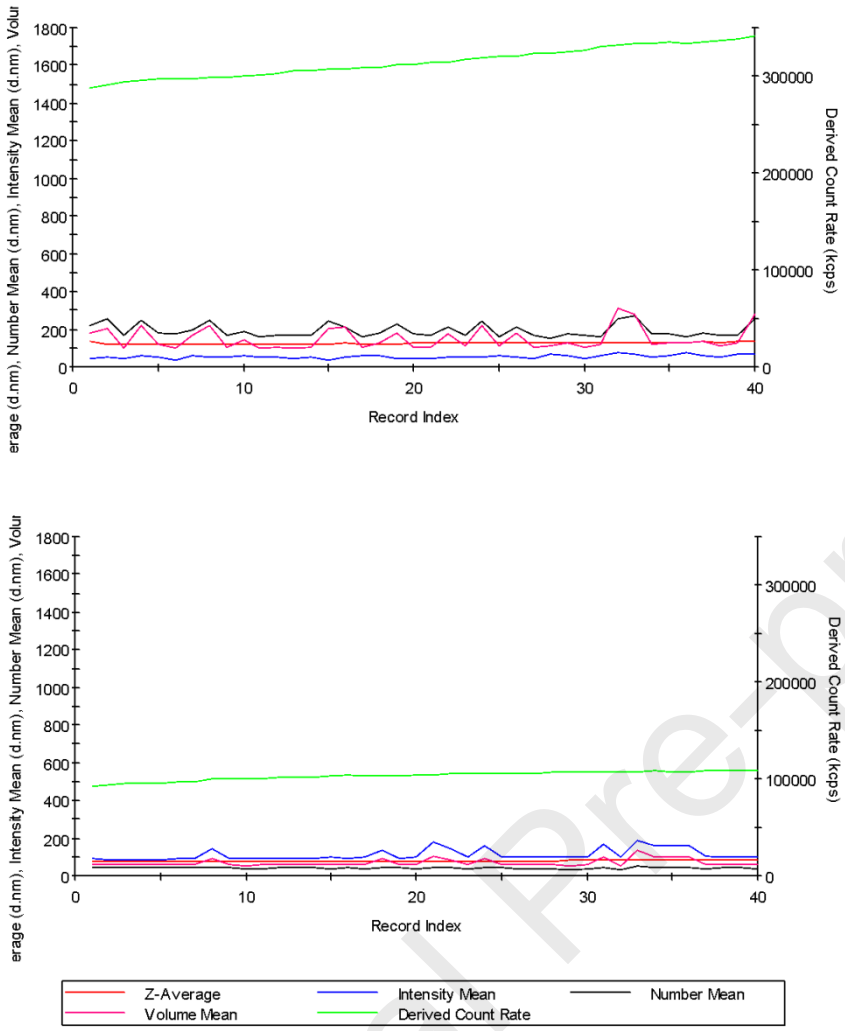

Figure 6. Size change over time of SLN incubated with isolated AP (top), control sample: SLN without isolated AP (middle), control SLN without phosphorylated PEG surfactant incubated with isolated AP (bottom). Left y-axis plotted Z-average mean size (d.nm), Intensity mean (d.nm), Number mean (d.nm) and Volume mean (d.nm). Right y-axis plotted derived count rate (kcps). Backscatter detection mode was used while measuring.

The presence of 0.5% PIC2 during incubation of SLN with isolated AP led also to the formation of aggregates. In contrast to the aggregation process without PIC2, however, this process took with around 6 h much longer. This result is in agreement with phosphate release studies shown in Figure 3 demonstrating that in the presence of 0.5% PIC2 phosphatase activity cannot be entirely inhibited.

SLN aggregation was probably the result of electrostatic interparticle interactions triggered by AP. An initial ZP of -45.4 (2.1) mV was obviously sufficiently high to repulse SLN form each other and to provide a stable dispersion. This is in agreement with numerous other studies showing that SLN with a ZP < -30 mV

are stable [33]. Due to the cleavage of phosphate substructures from the surface of SLN as shown in Figure 3, however, particles lose with the release of these anionic substructures their negative charge (Figure 4). As a consequence, the repulsion of SLN becomes too low to stabilize the system leading to SLN aggregation. Moreover, dephosphorylation of phosphorylated PEG surfactant would also disintegrate the 'phosphorylated PEG surfactant – octadecylamine' pseudo zwitterionic surfactant leading to the recovery of positively charged octadecylamine on SLN surface. This would contribute to a particle aggregation as octadecylamine on one SLN particle can electrostatically interact with phosphate groups that are still available on another SLN particle.

SLN aggregation occurred after ~30 min of incubation with isolated AP and seemed to flourish after ~50 min. The time required to initiate aggregation can be controlled by adjusting the amount of octadecylamine and/or phosphorylated PEG surfactant in SLN formulation. A SLN formulation with the same composition but lower amount of octadecylamine and phosphorylated PEG surfactant, i.e. 3 and 20 mg, respectively, had Z-average size of 121.7 (0.9) nm, PdI of 0.21 (0.01) and ZP of -17.9 (0.7) mV. The SLN was stable during storage for 48 h at room temperature. Upon incubation with isolated AP, aggregations appeared after 12 h, whereas control samples without isolated AP showed no size change.

Many research groups have exploited the concept of size-shifting nanoparticles for targeted drug delivery utilizing various trigger factors such as pH, UV light or temperature [34]. Na and Bae reported pullulan acetate-sulfadimethoxine hydrogel nanoparticles that can change their size upon exposure to the acidic tumoral pH. The size of nanoparticles was ~ 70 nm at pH ≥ 7.4 and increased to 1123 nm at pH ≤ 6.8 due to interparticle aggregation [35]. Photo-triggered size shifting of nanoparticles has been reported by Shi et al.. Nanoparticles constructed from bio-based photo-sensitive poly(4-cinnamic acid)-co-poly(3,4-cinnamic acid) increased in size by UV radiation at 254 nm due to a decrease in polymer crosslinking. Size could be reversibly decreased by radiation at > 280 nm due to polymer crosslinking [36]. Choi et al. prepared pluronic/poly (ethylenimine) nanocapsules that increased their size upon a short cold- shock treatment from ~100 nm at 37 °C to ~300 nm at 20 °C [37]. Amongst main mechanisms behind size-shifting

nanoparticles, i.e. reversible/irreversible swelling, particle aggregation and photo responsiveness, size shifting by aggregation seems to result in the most dramatic size change. Using an enzyme to trigger a size change of nanoparticles as described within this study is likely a new approach.

3.4. Drug release

Curcumin was loaded in SLN at an EE of 93.9 (0.4) %. As illustrated in Figure 7, SLN-C showed a sustained release of curcumin over time. Within 40 h around 30% of curcumin was recorded in the release medium. In the presence of isolated AP, SLN-C aggregation was observed and curcumin release was slower ($p < 0.05$) after 14-h time point compared to the release from samples without the presence of isolated AP. This might be explained by the formation of flocculation in samples with isolated AP that developed after particle aggregation. These flocs had much smaller total surface area and drug release rate was consequently slower.

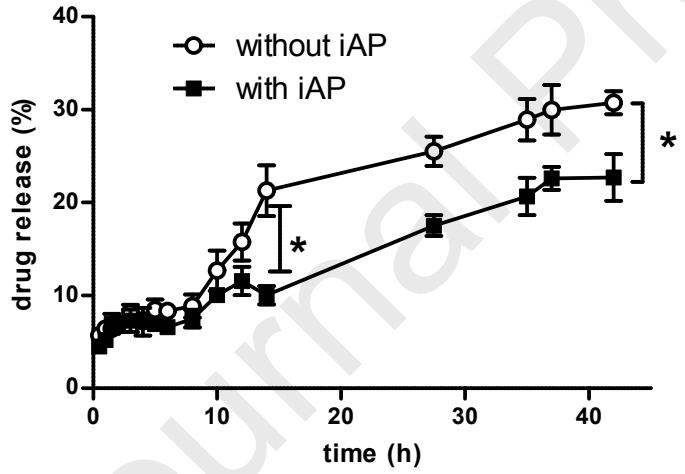

Figure 7. Curcumin release from SLN-C under the presence and absence of isolated AP. Indicated values are means and SDs (n=3), (*) $p < 0.05$. iAP = isolated AP.

3.5. SLN size changing on cell layers

Caco-2 cell line is frequently used as a model for the intestinal epithelial barrier as these cells express characteristics of enterocytes upon reaching confluence. Caco-2 cells have been shown to express human intestinal AP on their membrane [38]. Membrane bound AP cleaved phosphate from SLN in a similar

manner as the isolated enzyme. The presence of 0.5% PIC2 reduced the ability of the enzyme to cleave phosphate groups (Figure 8).

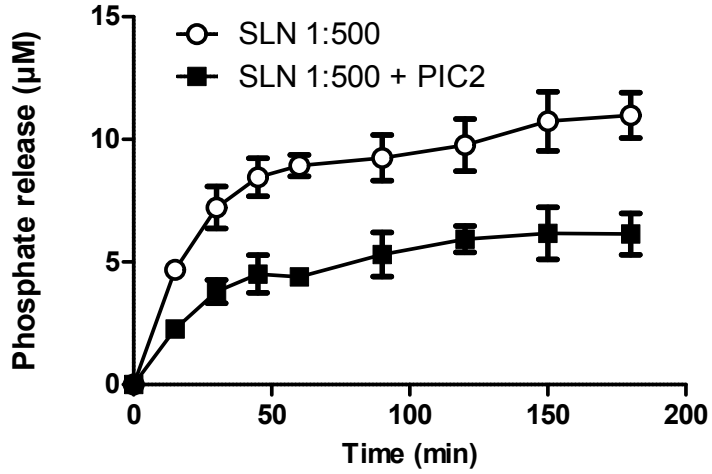

Figure 8. Phosphate release from SLN diluted 1:500 on Caco-2 cell layers in the absence and presence of 0.5% PIC2. Indicated values are means and SDs (n=3).

Incubating SLN on Caco-2 cell layer without mucus resulted in the formation of large SLN aggregates and internalization of SLN into cells as illustrated in Figure 9-1. When phosphatase inhibitors were present, less aggregation was observed, whereas more SLN were internalized into cells or accumulated in the region of tight junctions (Figure 9-2). This cellular uptake of SLN nanoparticles might have taken place directly after the AP-triggered change in ZP before the aggregation process was initiated. According to this observation, these SLNs might be useful to provide both fast and sustained drug release. Nano-size SLN could provide an immediate release or could be internalized into cells with their payload, whereas larger aggregates could in the following function as depot for a sustained drug release.

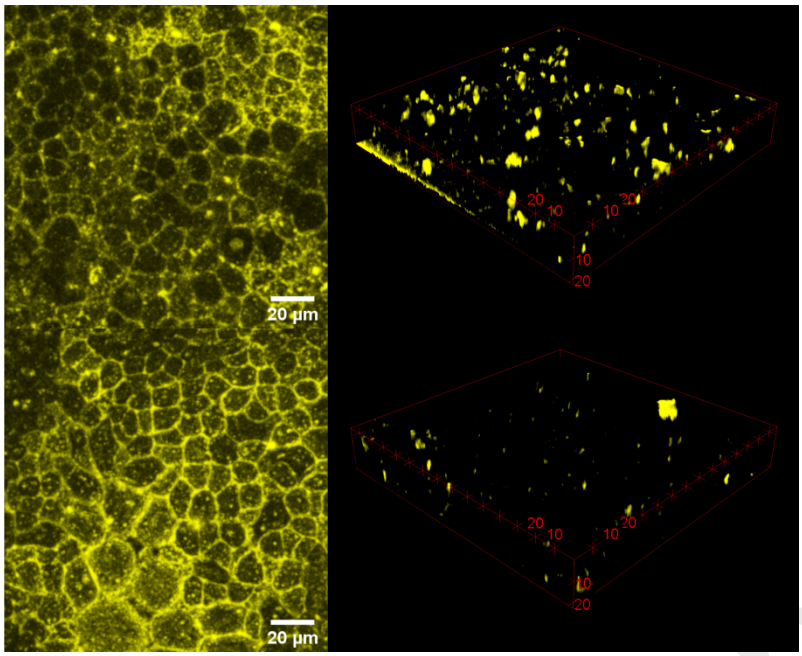

Figure 9. Confocal images of Caco-2 cell layers incubated with SLN in HBS (1) and in HBS containing phosphatase inhibitors (2). Images are means of 10 slices. On the right hand side are 3D representation of the segmented data (above cell layer), yellow clusters are SLN aggregates.

Mucus structure and thickness can vary on different mucosal tissues. In human GI tract, mucus gel is thickest in colon (50-300 µm [39], 480 (70) µm [40]) and stomach (144 (52) µm) and thin in small intestine (~15 µm) [41]. Mucus turnover along the human GI tract is between 24 and 48 h [41]. In lung, thickness of the mucus gel layer ranges from 7 µm in the deep airways to 55 µm in the bronchi [42]. Within this study, we utilized purified porcine mucus spread over the Caco-2 cell layer in order to investigate the impact of a mucus gel layer on the behavior of SLN. Mucus-secreting cell lines like HT29 MTX-E12 or A549 forming thin mucus layer of 3-5 µm [43] were not used in this study. Moreover, Lieleg et al. showed that incubation different cell lines with partially purified porcine mucin solution does not compromise cell viability [44].

Barr et al. investigated the diffusion behavior of phage particles with a size of 200 nm into a mucosal surface [45]. These particles first encountered the region of lowest mucin concentration and the most open mucin mesh. Close to the epithelium where mucin concentration increased, diffusivity decreased. More particles diffused from the outer mucus region into this firm mucus region close to the epithelium than diffused back out. The authors explained this observation by a temporary entrapment of these phage

particles in the firm mucus region. Particles smaller than 200 nm will likely to a higher extent diffuse into this firm mucus close to the epithelium. SLN with a mean size of ~120 nm permeated the mucus layer and reached the epithelium as shown in Figure 10. Nonetheless, aggregates were formed in the mucus on the epithelial surface that were less and smaller when phosphatase inhibitors were added (Figure 10C.1-2). Figure 11 illustrates the probability distribution of particles in the mucus layer in the absence and presence of phosphatase inhibitors. Mean size and SD of sample diluted in HBS was 681 (3.0401×10^3) pixel, while that of samples diluted in HBS containing phosphatase inhibitors was 498 (992) pixel. Looking at SD values, without phosphatase inhibitors, SLN particle size distributed over a wide range with the appearance of very large particles or aggregates. As large particles having been formed on the epithelial surface were trapped inside the mucus network due to their bulky size, their back-diffuse to the outer mucus layer is unlikely. Being immobilized in the mucus close to the absorption membrane, they can release their payload in a targeted manner. Moreover, microparticles were shown to accumulate and to remain in the mucosal wall at inflamed sites, while nanoparticles tend to be internalized and to induce systemic side effects [46]. Size-shifting feature has been utilized to disrupt endosomal membrane [37], to target tumors [35] and to trigger drug release [47]. Size-shifting nanoparticles offer the advantages of enhancing penetration and retention into tumors after extravasation [34]. Size-shifting SLN developed herein could therefore also be applied for site-specific mucosal drug delivery to colon, lung, vagina or mucus-secreting tumors where AP is frequently expressed.

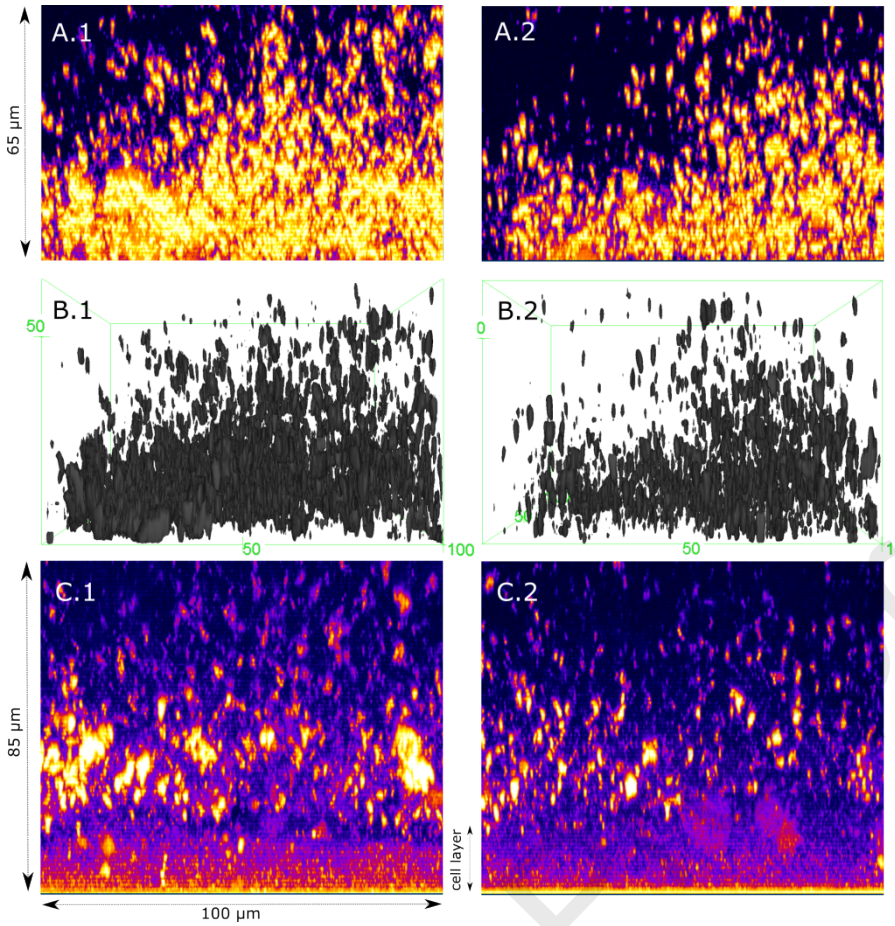

Figure 10. Processed confocal images of SLN on Caco-2 cell layers covered with purified porcine intestinal mucus: (1) SLN diluted in HBS, (2) SLN diluted in HBS containing 0.8% phosphatase inhibitors. A: XZ-maximum projection of segmented data above the cell layer. B: 3D representation of the segmented data (above cell layer). C: XZ-maximum projection of raw data including cell layer. Yellow clusters are SLN aggregates.

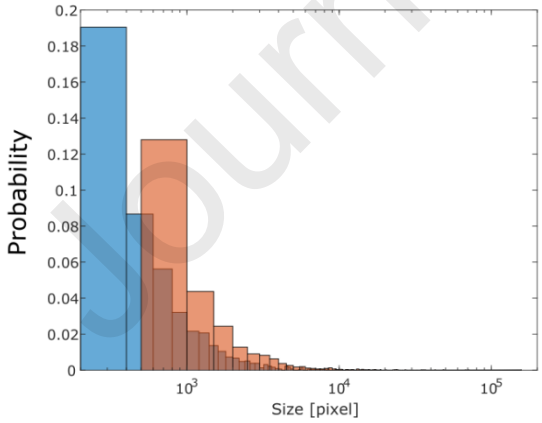

Figure 11. Probability size distribution of SLN aggregates in mucus layers. SLN was diluted in HBS (orange) and in HBS containing phosphatase inhibitors (blue).

4. Conclusion

We reported here for the first time about size-shifting SLN triggered by AP. SLN with a mean size of ~120 nm and a hydrophilic, negatively charged surface were shown to permeate the mucus gel layer, to reach the underlying epithelial surface and to form aggregates in the size of several microns. Phosphate removal from SLN surface by membrane bound AP lowered repulsion forces between particles and increased electrostatic interactions thus causing particle aggregation. Being trapped in the mucus gel network close to the absorption membrane due to their large size, these aggregates cannot back diffuse into outer mucus regions opening the door for site specific mucosal drug delivery to colon, lung, vagina, cervix or mucus-secreting tumors where AP is present.

Acknowledgment

B. Le-Vinh received a doctoral scholarship for the promotion of young researchers at the Leopold-Franzens-University Innsbruck.

References

[1] B.H. Bajka, N.M. Rigby, K.L. Cross, A. Macierzanka, A.R. Mackie, The influence of small intestinal mucus structure on particle transport ex vivo, Colloids Surfaces B Biointerfaces. 135 (2015) 73–80. doi:10.1016/j.colsurfb.2015.07.038.

[2] S.S. Olmsted, J.L. Padgett, A.I. Yudin, K.J. Whaley, T.R. Moench, R.A. Cone, Diffusion of Macromolecules and Virus-Like Particles in Human Cervical Mucus, Biophys. J. 81 (2001) 1930–1937. doi:https://doi.org/10.1016/S0006-3495(01)75844-4.

[3] X. Yang, K. Forier, L. Steukers, S. van Vlierberghe, P. Dubruel, K. Braeckmans, S. Glorieux, H.J. Nauwynck, Immobilization of Pseudorabies Virus in Porcine Tracheal Respiratory Mucus Revealed by Single Particle Tracking, PLoS One. 7 (2012). doi:10.1371/journal.pone.0051054.

[4] J.S. Crater, R.L. Carrier, Barrier Properties of Gastrointestinal Mucus to Nanoparticle Transport, Macromol. Biosci. 10 (2010) 1473–1483. doi:10.1002/mabi.201000137.

[5] M. Abdulkarim, P.K. Sharma, M. Gumbleton, Self-emulsifying drug delivery system: Mucus permeation and innovative quantification technologies, Adv. Drug Deliv. Rev. 142 (2019) 62–74. doi:10.1016/j.addr.2019.04.001.

[6] A. Mahmood, F. Laffleur, G. Leonaviciute, A. Bernkop-Schnürch, Protease-functionalized mucus penetrating microparticles: In-vivo evidence for their potential, Int. J. Pharm. 532 (2017) 177–184. doi:10.1016/j.ijpharm.2017.08.114.

[7] A. Macierzanka, N.M. Rigby, A.P. Corfield, N. Wellner, F. Böttger, E.N.C.C. Mills, A.R. Mackie, Adsorption of bile salts to particles allows penetration of intestinal mucus, Soft Matter. 7 (2011) 8077–8084. doi:10.1039/C1SM05888F.

[8] I. Pereira de Sousa, C. Steiner, M. Schmutzler, M.D. Wilcox, G.J. Veldhuis, J.P. Pearson, C.W. Huck, W. Salvenmoser, A. Bernkop-Schnurch, A. Bernkop-Schnürch, Mucus permeating carriers: formulation and characterization of highly densely charged nanoparticles, Eur J Pharm Biopharm. 97 (2015) 273–279. doi:10.1016/j.ejpb.2014.12.024.

[9] P. Blasi, S. Giovagnoli, A. Schoubben, M. Ricci, C. Rossi, Solid lipid nanoparticles for targeted brain drug delivery, Adv. Drug Deliv. Rev. 59 (2007) 454–477. doi:10.1016/j.addr.2007.04.011.

[10] R.H. Müller, K. Mäder, S. Gohla, Solid lipid nanoparticles (SLN) for controlled drug delivery, Eur. J. Pharm. Biopharm. 50 (2000) 161–77. doi:10.1080/026520499289185.

[11] E. Salah, M.M. Abouelfetouh, Y. Pan, D. Chen, S. Xie, Solid lipid nanoparticles for enhanced oral absorption: A review, Colloids Surfaces B Biointerfaces. 196 (2020) 111305. doi:10.1016/j.colsurfb.2020.111305.

[12] S. GuhaSarkar, R. Banerjee, Intravesical drug delivery: Challenges, current status, opportunities and novel strategies, J. Control. Release. 148 (2010) 147–159. doi:https://doi.org/10.1016/j.jconrel.2010.08.031.

[13] B. Le-Vinh, N.-M.N.N.-M.N. Le, I. Nazir, B. Matuszczak, A. Bernkop-Schnürch, Chitosan based micelle with zeta potential changing property for effective mucosal drug delivery, Int. J. Biol. Macromol. 133 (2019) 647–655. doi:10.1016/j.ijbiomac.2019.04.081.

[14] C.M. O'Driscoll, A. Bernkop-Schnürch, J.D. Friedl, V. Préat, V. Jannin, Oral delivery of non-viral nucleic acid-based therapeutics - do we have the guts for this?, Eur. J. Pharm. Sci. 133 (2019) 190–204. doi:10.1016/j.ejps.2019.03.027.

[15] T. Komoda, O. Nosjean, K. Honma, K. Nemoto, T. Sato, M. Miyanaga, H. Sugimoto, A Variant Alkaline Phosphatase Detected in a Patient with Lung Cancer, Enzym. Protein. 49 (1996) 313–320. doi:10.1159/000468641.

[16] D.C. Smith, W.B. Hunter, L.R. Spadoni, Alkaline Phosphatase Concentration in Cervical Mucus, Fertil. Steril. 21 (1970) 549–554. doi:10.1016/S0015-0282(16)37624-5.

[17] J.L. Millán, Alkaline Phosphatases- Structure, substrate specificity and functional relatedness to other members of a large superfamily of enzymes, Purinergic Signal. 2 (2006) 335–341. doi:10.1007/s11302-005-5435-6.

[18] W. Suchaoin, I. Pereira de Sousa, K. Netsomboon, H.T. Lam, F. Laffleur, A. Bernkop-Schnurch, A. Bernkop-Schnürch, Development and in vitro evaluation of zeta potential changing self-emulsifying drug delivery systems for enhanced mucus permeation, Int. J. Pharm. 510 (2016) 255–262. doi:10.1016/j.ijpharm.2016.06.045.

[19] J.D. Wolf, M. Kurpiers, R.X. Götz, S. Zaichik, A. Hupfauf, D. Baecker, R. Gust, A. Bernkop-Schnürch, Phosphorylated PEG-emulsifier: Powerful tool for development of zeta potential changing self-emulsifying drug delivery systems (SEDDS), Eur. J. Pharm. Biopharm. 150 (2020) 77–86. doi:10.1016/j.ejpb.2020.03.004.

[20] E. Salimi, B. Le-Vinh, F. Zahir-Jouzdani, B. Matuszczak, A. Ghaee, A. Bernkop-Schnürch, A. Bernkop-Schnurch, Self-emulsifying drug delivery systems changing their zeta potential via a flip-flop mechanism, Int. J. Pharm. 550 (2018) 200–206. doi:10.1016/j.ijpharm.2018.08.046.

[21] H. Friedl, S. Dünnhaupt, F. Hintzen, C. Waldner, S. Parikh, J.P. Pearson, M.D. Wilcox, A. Bernkop-Schnürch, Development and evaluation of a novel mucus diffusion test system approved by self-nanoemulsifying drug delivery Systems, J. Pharm. Sci. 102 (2013) 4406–4413. doi:10.1002/jps.23757.

[22] A. Macierzanka, N.M. Rigby, A.P. Corfield, N. Wellner, F. Böttger, E.N.C.C. Mills, A.R. MacKie, Adsorption of bile salts to particles allows penetration of intestinal mucus, Soft Matter. 7 (2011) 8077–8084. doi:10.1039/c1sm05888f.

[23] A. Siddiqui, A. Alayoubi, Y. El-Malah, S. Nazzal, Modeling the effect of sonication parameters on size and dispersion temperature of solid lipid nanoparticles (SLNs) by response surface methodology (RSM), Pharm. Dev. Technol. 19 (2014) 342–346. doi:10.3109/10837450.2013.784336.

[24] W. Mehnert, K. Mäder, Solid lipid nanoparticles: Production, characterization and applications, Adv. Drug Deliv. Rev. 64 (2012) 83–101. doi:10.1016/j.addr.2012.09.021.

[25] T.F. Tadros, Emulsion Formation, Stability, and Rheology, in: T.F. Tadros (Ed.), Emuls. Form. Stab., 1st ed., Wiley-VCH Verlag GmbH & Co. KGaA., 2013: pp. 1–76. doi:10.1002/9783527647941.ch1.

[26] B.K. Paul, S.P. Moulik, Structure, dynamics and transport properties of microemulsions, Adv. Colloid Interface Sci. 78 (1998) 99–195. doi:10.1016/S0001-8686(98)00063-3.

[27] C. Grapentin, C. Müller, R.S.K. Kishore, M. Adler, I. ElBialy, W. Friess, J. Huwyler, T.A. Khan, Protein-Polydimethylsiloxane Particles in Liquid Vial Monoclonal Antibody Formulations Containing Poloxamer 188, J. Pharm. Sci. 109 (2020) 2393–2404. doi:10.1016/j.xphs.2020.03.010.

[28] S.M. Moghimi, A.C. Hunter, C.M. Dadswell, S. Savay, C.R. Alving, J. Szebeni, Causative factors behind poloxamer 188 (Pluronic F68, Flocor™)-induced complement activation in human sera: A protective role against poloxamer-mediated complement activation by elevated serum lipoprotein levels, Biochim. Biophys. Acta - Mol. Basis Dis. 1689 (2004) 103–113. doi:https://doi.org/10.1016/j.bbadis.2004.02.005.

[29] P. Alexandridis, T.A. Hatton, Poly (ethylene oxide)poly (propylene oxide)poly (ethylene oxide) block copolymer surfactants in aqueous solutions and at interfaces: thermodynamics, structure, dynamics, and modeling, Colloids Surfaces A Physicochem. Eng. Asp. 96 (1995) 1–46.

[30] G. Kume, M. Gallotti, G. Nunes, Review on anionic/cationic surfactant mixtures, J. Surfactants Deterg. 11 (2008) 1–11. doi:10.1007/s11743-007-1047-1.

[31] N. El Kadi, F. Martins, D. Clausse, P.C. Schulz, Critical micelle concentrations of aqueous hexadecytrimethylammonium bromide-sodium oleate mixtures, Colloid Polym. Sci. 281 (2003) 353–362. doi:10.1007/s00396-002-0783-z.

[32] B.T. Burlingham, T.S. Widlanski, Synthesis and biological activity of N-sulfonylphosphoramidates: Probing the electrostatic preferences of alkaline phosphatase, J. Org. Chem. 66 (2001) 7561–7567. doi:10.1021/jo010495q.

[33] N. Raval, R. Maheshwari, D. Kalyane, S.R. Youngren-Ortiz, M.B. Chougule, R.K. Tekade, Chapter 10 - Importance of Physicochemical Characterization of Nanoparticles in Pharmaceutical Product Development, in: R.K.B.T.-B.F. of D.D. Tekade (Ed.), Adv. Pharm. Prod. Dev. Res., Academic Press, 2019: pp. 369–400. doi:https://doi.org/10.1016/B978-0-12-817909-3.00010-8.

[34] J.W. Yoo, N. Doshi, S. Mitragotri, Adaptive micro and nanoparticles: Temporal control over carrier properties to facilitate drug delivery, Adv. Drug Deliv. Rev. 63 (2011) 1247–1256. doi:10.1016/j.addr.2011.05.004.

[35] K. Na, Y.H. Bae, Self-assembled hydrogel nanoparticles responsive to tumor extracellular pH from pullulan derivative/sulfonamide conjugate: characterization, aggregation, and adriamycin release in vitro., Pharm. Res. 19 (2002) 681–688. doi:10.1023/a:1015370532543.

[36] D. Shi, M. Matsusaki, T. Kaneko, M. Akashi, Photo-Cross-Linking and Cleavage Induced Reversible Size Change of Bio-Based Nanoparticles, Macromolecules. 41 (2008) 8167–8172. doi:10.1021/ma800648e.

[37] S.H. Choi, S.H. Lee, T.G. Park, Temperature-sensitive pluronic/poly(ethylenimine) nanocapsules for thermally triggered disruption of intracellular endosomal compartment., Biomacromolecules. 7 (2006) 1864–1870. doi:10.1021/bm060182a.

[38] H. Matsumoto, R.H. Erickson, J.R. Gum, M. Yoshioka, E. Gum, Y.S. Kim, Biosynthesis of Alkaline-Phosphatase During Differentiation of the Human Colon Cancer Cell-Line Caco-2, Gastroenterology. 98 (1990) 1199–1207. doi:10.1016/0016-5085(90)90334-W.

[39] R.D. Pullan, G.A.O. Thomas, M. Rhodes, R.G. Newcombe, G.T. Williams, A. Allen, J. Rhodes, Thickness of adherent mucus gel on colonic mucosa in humans and its relevance to colitis, Gut. 35

(1994) 353–359. doi:10.1136/gut.35.3.353.

[40] J.K. Gustafsson, A. Ermund, M.E.V. Johansson, A. Schütte, G.C. Hansson, H. Sjövall, An ex vivo method for studying mucus formation, properties, and thickness in human colonic biopsies and mouse small and large intestinal explants, Am. J. Physiol. - Gastrointest. Liver Physiol. 302 (2012) 430–438. doi:10.1152/ajpgi.00405.2011.

[41] F. Taherali, F. Varum, A.W. Basit, A slippery slope : On the origin , role and physiology of mucus, Adv. Drug Deliv. Rev. 124 (2018) 16–33. doi:10.1016/j.addr.2017.10.014.

[42] A.S. Verkman, Y. Song, J.R. Thiagarajah, Role of airway surface liquid and submucosal glands in cystic fibrosis lung disease., Am. J. Physiol. Cell Physiol. 284 (2003) C2-15. doi:10.1152/ajpcell.00417.2002.

[43] J.Y. Lock, T.L. Carlson, R.L. Carrier, Mucus models to evaluate the diffusion of drugs and particles, Adv Drug Deliv Rev. 124 (2018) 34–49. doi:10.1016/j.addr.2017.11.001.

[44] O. Lieleg, C. Lieleg, J. Bloom, C.B. Buck, K. Ribbeck, Mucin Biopolymers As Broad-Spectrum Antiviral Agents, Biomacromolecules. 13 (2012) 1724–1732. doi:10.1021/bm3001292.

[45] J.J. Barr, R. Auro, N. Sam-Soon, S. Kassegne, G. Peters, N. Bonilla, M. Hatay, S. Mourtada, B. Bailey, M. Youle, B. Felts, A. Baljon, J. Nulton, P. Salamon, F. Rohwer, Subdiffusive motion of bacteriophage in mucosal surfaces increases the frequency of bacterial encounters, Proc. Natl. Acad. Sci. U. S. A. 112 (2015) 13675–13680. doi:10.1073/pnas.1508355112.

[46] C. Schmidt, C. Lautenschlaeger, E.M. Collnot, M. Schumann, C. Bojarski, J.D. Schulzke, C.M. Lehr, A. Stallmach, Nano- and microscaled particles for drug targeting to inflamed intestinal mucosa - A first in vivo study in human patients, J. Control. Release. 165 (2013) 139–145. doi:10.1016/j.jconrel.2012.10.019.

[47] W. Chen, F. Meng, R. Cheng, Z. Zhong, pH-Sensitive degradable polymersomes for triggered release of anticancer drugs: A comparative study with micelles, J. Control. Release. 142 (2010) 40–46. doi:https://doi.org/10.1016/j.jconrel.2009.09.023.